AFRL-AFOSR-VA-TR-2020-0192

Sub-Diffraction Temperature Mapping of Protein Interconversions

Somin Eunice Lee
REGENTS OF THE UNIVERSITY OF MICHIGAN

09/15/2020
Final Report

Air Force Research Laboratory
AF Office Of Scientific Research (AFOSR)/ RTB2
Arlington, Virginia 22203
Air Force Materiel Command

REPORT DOCUMENTATION PAGE

Form Approved
OMB No. 0704-0188

1. REPORT DATE *(DD-MM-YYYY)*	2. REPORT TYPE	3. DATES COVERED *(From - To)*
13-10-2020	Final Performance	15 May 2016 to 14 May 2020

4. TITLE AND SUBTITLE
Sub-Diffraction Temperature Mapping of Protein Interconversions

5a. CONTRACT NUMBER

5b. GRANT NUMBER
FA9550-16-1-0272

5c. PROGRAM ELEMENT NUMBER
61102F

6. AUTHOR(S)
Somin Eunice Lee

5d. PROJECT NUMBER

5e. TASK NUMBER

5f. WORK UNIT NUMBER

7. PERFORMING ORGANIZATION NAME(S) AND ADDRESS(ES)
REGENTS OF THE UNIVERSITY OF MICHIGAN
503 THOMPSON ST
ANN ARBOR, MI 48109-1340 US

8. PERFORMING ORGANIZATION REPORT NUMBER

9. SPONSORING/MONITORING AGENCY NAME(S) AND ADDRESS(ES)
AF Office of Scientific Research
875 N. Randolph St. Room 3112
Arlington, VA 22203

10. SPONSOR/MONITOR'S ACRONYM(S)
AFRL/AFOSR RTB2

11. SPONSOR/MONITOR'S REPORT NUMBER(S)
AFRL-AFOSR-VA-TR-2020-0192

12. DISTRIBUTION/AVAILABILITY STATEMENT
A DISTRIBUTION UNLIMITED: PB Public Release

13. SUPPLEMENTARY NOTES

14. ABSTRACT
The ability to spatially and temporally map nanoscale environments would be highly transformative for revealing dynamic biophysical phenomena. As investigations of time-dependent processes demand broad time observation windows previously unreachable by fluorescence super-resolution, a nonbleaching strategy is needed. We developed precision optics to suppress errors required for subdiffraction imaging. We scaled this method to unlimited numbers of scatterers. With a nonbleaching subdiffraction approach capable of broad timescales, we followed the temporal evolution of actin materials with subdiffraction resolution over broad time periods.

15. SUBJECT TERMS
protiens, sub-diffraction thermal mapping, protein interconversions, nano-antennas

16. SECURITY CLASSIFICATION OF:			17. LIMITATION OF ABSTRACT	18. NUMBER OF PAGES	19a. NAME OF RESPONSIBLE PERSON
a. REPORT	b. ABSTRACT	c. THIS PAGE			BIN-SALAMON, SOFI
Unclassified	Unclassified	Unclassified	UU		19b. TELEPHONE NUMBER *(Include area code)* 703-696-8411

Standard Form 298 (Rev. 8/98)
Prescribed by ANSI Std. Z39.18

COVERPAGE

Subject: Final Report to Dr. Bin-Salamon

Contract/Grant Title: Sub-diffraction temperature mapping of protein interconversions

Contract/Grant #: FA9550-16-1-0272

Reporting Period: May 14, 2016 – May 14, 2020

ABSTRACT

The ability to spatially and temporally map nanoscale environments would be highly transformative for revealing dynamic biophysical phenomena. To this end, broad timescales require time-resolved analysis while local rearrangements of nanoscale environments necessitate spatial super-resolution, juxtaposing the requirement for time resolution with the need for spatial resolution. To achieve spatial resolution below the diffraction limit, a common approach is to use fluorescence super-resolution that utilizes activation and/or deactivation of fluorophores until fluorophores eventually irreversibly photobleach, precluding temporally demanding endeavors. Thus, high spatial resolution comes at a cost to temporal capabilities. As investigations of time-dependent processes demand broad time observation windows previously unreachable by fluorescence super-resolution, a nonbleaching strategy is needed (Figure 1). Unlike fluorophores, plasmonic scatterers do not photobleach. To enhance spatial resolution, scattering can be modulated using polarization. In this way, plasmonic nanoscatterers which scatter with different polarization states of light can be localized. However, all aforementioned demonstrations have been so far constrained to one to few nanoscatterers, in which such limited numbers are insufficient for imaging macroscale materials. We developed precision optics to suppress errors required for subdiffraction imaging. We scaled this method to unlimited numbers of scatterers. With a nonbleaching subdiffraction approach capable of broad timescales, we followed the temporal evolution of actin materials with subdiffraction resolution over broad time periods. Finally, we quantified biophysical (*e.g.*, degradation rates, temperature) by nonbleaching nanoscopy.

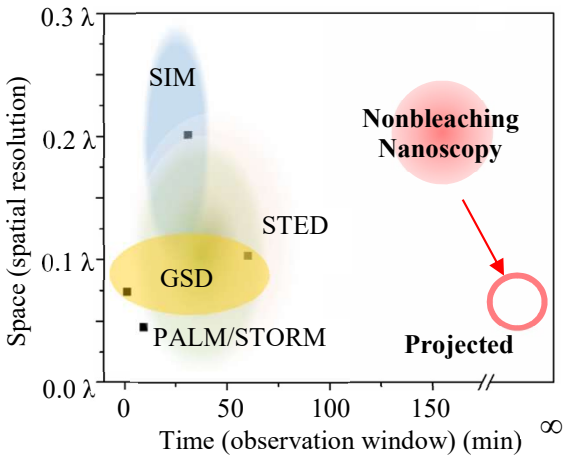

Figure 1. Nonbleaching nanoscopy for revealing dynamic biophysical phenomena. (a) Super-resolution methods, ground state depletion (GSD), stimulated emission depletion (STED), structured illumination microscopy (SIM), photo-activated localization microscopy (PALM), and stochastic optical reconstruction microscopy (STORM), have pushed spatial resolution beyond the diffraction limit. To push the current limits of time observation windows, nonbleaching nanoscopy is insusceptible to photobleaching and enables new biophysical studies across the time continuum.

OBJECTIVES

- Develop precision optics to suppress errors required for nonbleaching nanoscopy.
- Confirm optically and structurally stabilized interlinking networks in potential applications as active/responsive materials.
- Scale nonbleaching nanoscopy from few scatterers to unlimited numbers of scatterers.

- Demonstrate nonbleaching nanoscopy with subdiffraction resolution over broad time periods.
- Quantify subdiffraction biophysical parameters (*e.g.*, degradation rates, temperature) by nonbleaching nanoscopy.

ACCOMPLISHMENTS

Precision Optics

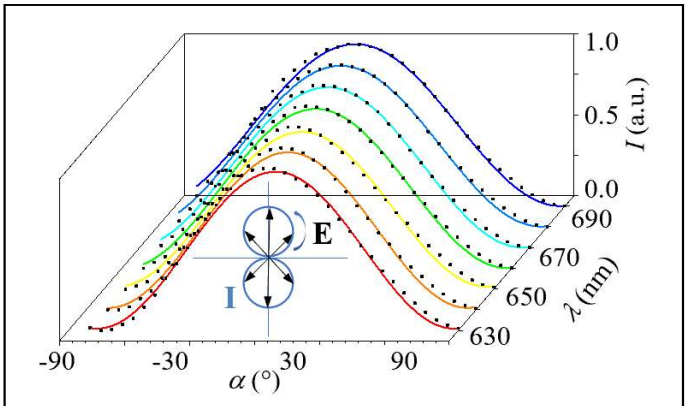

Figure 2. Precision optics: Polarizer. Characterization of device operation. Transmission intensity vs. angle α across wavelengths λ following Malus's Law. Angle α is between the transmission axes of the device and a fixed linear polarizer.

Optical manipulation and imaging of nano-objects with nanometer precision is highly desirable for biological studies due to inherent noninvasiveness. However, current segregated experimental systems for nanoimaging and nanomanipulation limits real-time super-resolution imaging with control. We developed an integrated nanoscopic correction (iNC) method to enable multimodal nanomanipulation-nanoimaging. The iNC consists of a multimodal voltage-tunable power modulator, polarization rotator, and polarizer. Using iNC, we demonstrate scatterers (gold nanorods) which are below diffraction limit can be distinguished by direct observation without post processing. Furthermore, we show such direct observations with 100 times enhanced nanometer spatial stability and millisecond high speed. We successfully demonstrate precise trapping and rapid rotation of scatterers with iNC. We anticipate iNC will make contributions in the biological sciences requiring precision optics.

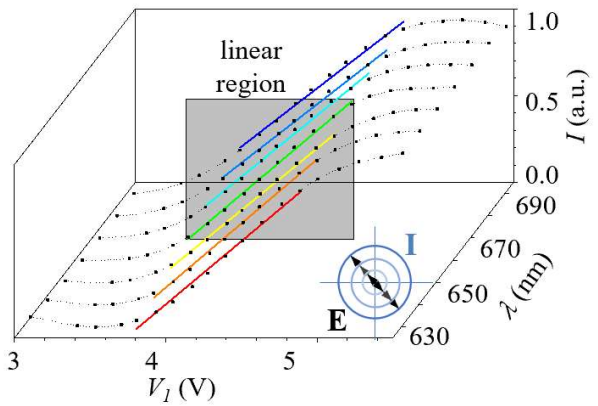

Figure 3. Precision optics: Power modulator. Characterization of device operation. Transmission intensity as a function of actuation voltage V_1 across wavelengths λ.

The iNC in the polarizer mode enables imaging of scatterers (Figure 2). We imaged single nanocrystals (gold nanorods) over a range of polarization θ from 0° to 180°. When a conventional polarizer was used to rotate the polarization from 0° to 180°, the Airy patterns of the imaged nanocrystals followed a spiral trace exhibiting a sin(θ/2) behavior due to a non-zero angle between the two surfaces of the rotating optics and due to an offset between the rotating axis of the rotation mount and the axis of the optics. The maximum spatial error (diameter traced by the

nanorod image trajectory) was as large as 1300 nm. For quantitative characterization, the root-mean-square deviation (RMSD) of each pixel was calculated between the intensity of the pixels and a fitted sinusoidal function. With a conventional polarizer, large RMSD was observed due to spatial errors across pixels and subsequent loss of spatial information from finite CCD sampling. Such spatial errors far exceed the diameter of Airy patterns. When spatial errors reach the same size order of the Airy patterns, positional information is substantially obscured and direct visualization of the proximal nanocrystals from their far-field Airy patterns becomes impossible. In contrast, we observed the Airy patterns of imaged nanocrystals remained at their same positions over the entire range of polarization using the iNC. We observed small RMSD with the iNC, indicating a better fit to sinusoidal functions as a result of sub-pixel spatial stability. Notably, suppression of spatial errors gives rise to accurate and precise spatial information, allowing us to directly observe and distinguish segregated Airy patterns of proximal nanocrystals without any spatial image corrections. For a single nanocrystal, its Airy pattern remained at the same position. When we imaged proximal nanocrystals, Airy patterns corresponding to each nanocrystal emerged. Nanometer positions were directly observed without image post-processing. We concluded the iNC permits proximal nanocrystals to be directly distinguished beyond the diffraction limit.

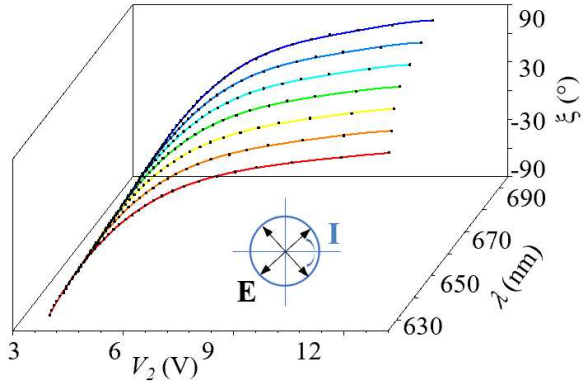

Figure 4. Precision optics: Polarization rotator. Characterization of device operation. Polarization rotation angle ξ as a function of actuation voltage V_2 across wavelengths λ.

The iNC in the power modulator mode (Figure 3) and polarization rotator mode (Figure 4) enable manipulation of scatterers. For optical trapping, we modulated the trapping power from 30 mW to 90 mW using the iNC in the power modulator mode. The scatterer position was measured using a quadrant photodiode to obtain its positional probability distribution. As a scatterer in solution undergoes Brownian motion even when optically trapped, the trapping force must overcome the Brownian motion in order for the scatterer to be stably trapped. We observed higher trapping powers resulted in more confined spatial distributions, demonstrating scatterers can be stably trapped using the iNC. Trapped nanocrystals can be then actively controlled to rotate using the iNC in the polarization rotator mode. A scatterer will tend to align along the light incident polarization. Thus, a trapped scatterer will rotate following the polarization direction. By tuning the voltage of the iNC, the linearly polarized trapping beam changed its polarization direction, causing the trapped scatterer to rotate. Using a polarizer/analyzer technique, the intensity of the rotating scatterer (gold nanorod) after a fixed analyzer was recorded with CCD. We observed that the intensity was lowest when the scatterer rotated to the position perpendicular to the analyzer and highest when the scatterer fully aligned with the analyzer.

Optically and structurally stabilized interlinking networks

Interlinking networks, such as the cytoskeleton, dynamically respond and adapt to the constantly changing environment. Detailed visualization of the complex dynamics of interlinking networks would be highly beneficial in developing composite materials and active/responsive materials. However, conventional light microscopy yields limited resolution, owing to light diffraction, for visualizing complex dynamics of interlinking networks. In contrast, scatterers are not susceptible to photobleaching, making them potential candidates as visualization probes for dynamic interlinking networks. Proximal scatterers can be spectrally or temporally isolated within interlinking networks under the condition that nanostructures maintain their plasmonic properties. Thus, three requirements must be fulfilled: 1) CTA+ free, 2) structurally stable under physical, chemical and biological environments, and 3) efficient crosslinking with interlinking networks.

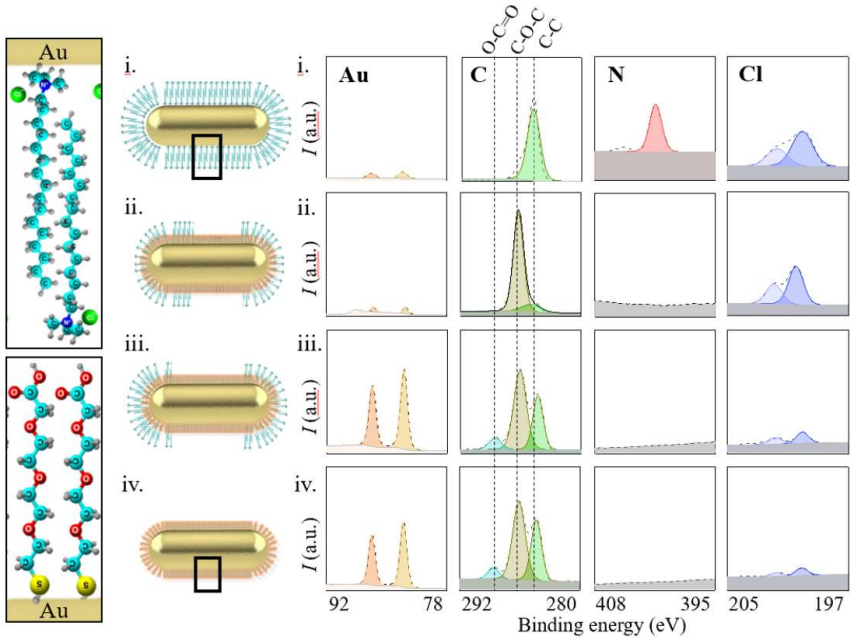

Figure 5. CTA+ free scatterers are the foundation for stable interlinking networks. (left) Conceptual schematic before and after synthesis of CTA+ free BioAuNRs. (right) Synthetic steps and corresponding XPS spectra to achieve CTA+ free scatterers. i. $n_{sw} = 0$, ii. $n_{sw} = 1$, iii. $n_{sw} = 10$, iv. $n_{sw} = 20$ where n_{sw} is the number of surface washings.

Achieving CTA+ free prepares the essential foundation for visualizing dynamic interlinking networks. Traditionally, scatterers (gold nanorods) are synthesized with a strong cationic charge from hexadecyltrimethylammonium bromide (CTAB) capping, which can impact subsequent ligand exchange. We developed an alternative bromide-free method to achieve CTA+ free using hexadecyltrimethylammonium chloride (CTAC). Ligand exchange was conducted by adapting a round trip ligand exchange approach for CTAC scatterers. To quantitatively assess that scatterers were indeed CTA+ free, high resolution X-ray photoelectron spectroscopy (XPS) was conducted (Figure 5). These results show that CTAC can be completely removed to yield CTA+ free scatterers. To the best of our knowledge, all existing ligand exchange protocols focus on the removal of CTAB. In this work, complete ligand exchange of CTAC - indicated by the absence of

nitrogen N 1s originating from CTAC - can be achieved to yield CTA+ free scatterers, laying the foundation for stable interlinked networks.

We developed a new stability algorithm, referred to as the comprehensive stability parameter (CSP), to quantitatively and comprehensively analyze stability. Traditionally, to estimate the stability of plasmonic nanostructures, spectral features, such as the change of the peak extinction rate, shift of the resonant peak, change of the extinction ratio at 400 and 800 nm (A400/ A800), aggregation index, and ratio of the longitudinal surface plasmon resonance to the transverse surface plasmon resonance, have been used. However, most approaches rely on only on a single spectral feature and/or a subset of spectral features, thereby achieving limited results on the overall structural and optical stability of plasmonic nanostructures. Particularly, these limitations have implications on complicated geometries, such as interlinked networks. In contrast, CSP incorporates the entire spectrum to avoid potential bias from a single spectral feature and/or a subset of spectral features. Because CSP captures changes across the entire spectra, gradual and minimal instability not detectable with the conventional method can be detected. Furthermore, CSP may be used in classifying stability into five groups: highly stable (CSP≥0.75), stable (0.5≤CSP<0.75), semi-stable (0.25≤CSP<0.5), unstable (CSP<0.25), and highly unstable (CSP≈0). We found that efficient crosslinking could be achieved with CTA+ free scatterers of 0.82 CSP, whereas interlinking networks poorly formed with 0.16 CSP.

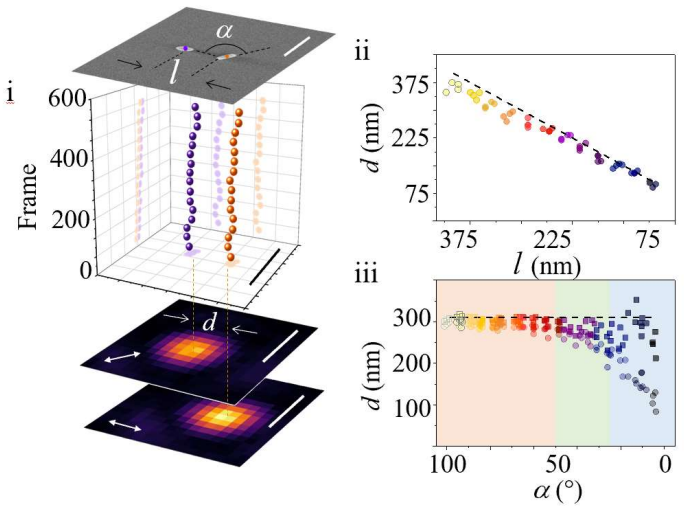

Figure 6. Nonbleaching subdiffraction localization. Scanning electron microscopy image of a pair of scatterers (gold nanorods). Scale bar: 220 nm. Airy patterns precisely correspond to nanometer positions of each scatterer. Scale bar: 520 nm. Scatter plot constructed from stacks of Airy patterns. Scale bar: 925 nm. ii. Localization distance *d* versus measured distance *ℓ* by scanning electron microscopy. Colored circles represent replicates of n = 4, where n is the number of replicates per group. Dashed line represents the average distance. iii. Localization distance *d* as orientation *α* is varied. Colored circles (algorithm 1) represent replicates of n = 4. Colored squares (algorithm 2) represent replicates of n = 4.

High crosslinking efficiency is necessary for super-resolution imaging. We demonstrated optically and structurally stable PBIN exhibiting 100% CTA+ free and 97% crosslinking efficiencies. With interlinking networks exhibiting 97% crosslinking efficiencies, darkfield microscopy images show CTA+ free scatterers uniformly assembled along the network, allowing fine structural features of the network to be clearly visualized. Intensity profiles show several peaks with low background, indicating individual CTA+ free scatterers were well separated and high signal-to-noise ratio can be achieved. Computed electric field distributions confirmed individual plasmonic properties were preserved. In contrast, poor crosslinking resulted in

aggregated assemblies such that network structural details could not be visualized. Computed electric field distributions showed individual plasmonic properties were lost in the case of poor crosslinking. Large background contributed to the small signal-to-noise ratio and degraded the imaging quality, impeding super-resolution imaging capabilities.

After establishing structural stability, we studied the optical stability of interlinking networks. Actin is well-known to depolymerize by removing subunits at its polymer ends, and such dynamics gives rise to cytoskeletal reorganization and motility. Whereas many studies have been conducted on the short term dynamics of actin, little is known about the long term dynamic properties of actin depolymerization. This is due in part because of current technological limitations in long term, continuous imaging capabilities. With long term, continuous capabilities, we studied the depolymerization process. Interlinking slowly depolymerized over ~360 min and disappeared after 450 min. Such long term dynamics cannot be captured in fluorescent interlinking networks. As an active/responsive material, we studied interlinking networks in response to optical stimulus. We were able to observe ~200 - 300 nm displacements using remotely controlled, focused λ = 730 nm, 9 mW CW laser light. Using on-resonance wavelength (730 nm) and off-resonance resonant wavelength (930 nm), displacements as a function of illumination power were reversible, showing the potential of interlinking networks as an active/responsive material.

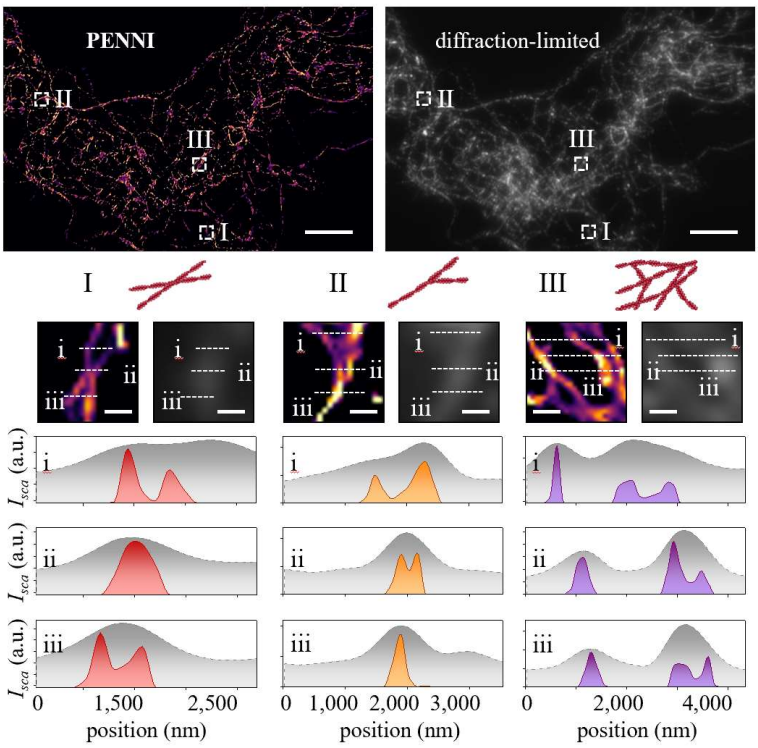

Figure 7. Nonbleaching nanoscopy (PENNI) is scalable. Images of actin networks: PENNI-resolved (left side), diffraction-limited (right side). Representative architecturally distinct actin structures are boxed and magnified in part c. Scale bar 10 μm. (left) Intersected actin structure with corresponding line profiles. (middle) Branched actin structure with corresponding line profiles. (right) Complex actin structure with corresponding line profiles. Scale bar: 734 nm.

Nonbleaching nanoscopy

As a first test of subdiffraction localization, we considered a pair of nanorods as a model of proximal nonbleaching scatterers (Figure 6). Using precision optics, we directly observed that the position of the Airy pattern at the imaging plane precisely corresponded to the positions of each scatterer without any spatial image correction. Localization can be optimized based on aspect

ratio. Notably, we highlight that localization with nanometer accuracy is achievable with precision optics. As the polarization-dependent transmission intensity was modulated, image stacks were acquired in order to observe a sufficient number of localization events to resolve the underlying spatial positions. By analyzing the acquired image stacks, distinct populations corresponded to each distinct scatterer from which spatial positions were quantified. In contrast, under conventional diffraction limited imaging, a single Airy pattern appeared at the imaging plane and therefore the individual scatterers could not be distinguished.

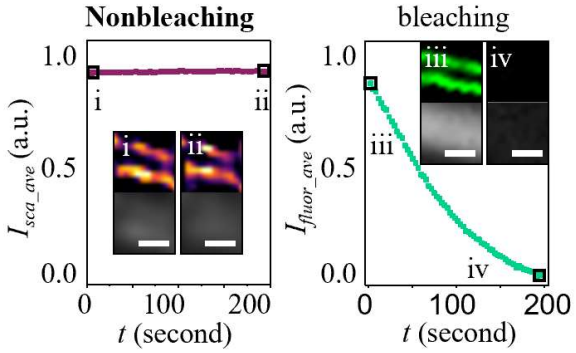

Figure 8. Nonbleaching nanoscopy is insusceptible to photobleaching. PENNI-resolved image at time t = 0 sec (top), diffraction-limited image at time t = 0 sec (bottom). ii. PENNI-resolved image at time t = 200 sec (top), diffraction-limited image at time t = 200 sec (bottom). Graph of average fluorescence intensity over time (green). Inset: iii. Fluorescence super-resolution resolved image at time t = 0 sec (top), diffraction-limited image at time t = 0 sec (bottom). iv. Fluorescence super-resolution resolved image at time t = 200 sec (top), diffraction-limited image at time t = 200 sec (bottom). Scale bar: 725 nm.

To validate localization accuracy, we investigated pairs of scatterers separated by varying subdiffraction distances and compared with measurements by scanning electron microscopy. Distances d obtained by subdiffraction localization agree well with distances l obtained by scanning electron microscopy, within an uncertainty of ±3.5 nm, which is well below the size order of scatterers. Next, we investigated pairs of scatterers separated by subdiffraction distance but with varying orientations α. When orientations differed by $\alpha \sim 50°$, scatterers can be clearly localized with high resolution. When the orientation was similar ($\alpha \sim 25°$), scatterers can still be localized. This can be further improved using alternative localization algorithms. For example, very similar orientations ($\alpha \sim 5°$) can be localized with alternative localization algorithms.

We next scaled up to spatially resolve n number of nanoscatterers, a technique termed here as polarization enabled nonbleaching nanoscopic imaging (PENNI). Scatterers were incorporated into actin material. Precision optics were employed to modulate their polarization-dependent transmission intensity as multiframe images were acquired. Using our new method PENNI, we were able to scalably resolve from 2 scatterers (Figure 6) to 3,978 scatterers (Figure 7). By extracting the line profiles at locations in the actin material, the diameter of a bundle was measured to be 136nm using PENNI in comparison to 816 nm by diffraction-limited imaging, demonstrating that bundles were crisper and more defined using PENNI. Subdiffraction PENNI images clearly show details of architecturally distinct structures which are indistinguishable in the diffraction-limited images. Detailed structures of intersected bundles were distinguishable by PENNI. Multiple line profiles along the PENNI-resolved structure clearly show that the intersected bundles initially converge, then intersect, and finally diverge again which cannot be seen in the diffraction-limited image. Branched structures were also visible by PENNI. Line profiles along the PENNI-resolved structure show a daughter bundle protruded from the side of a mother bundle, forming a Y-shaped branch that is undetectable in the diffraction-limited image. Finally, higher ordered

structures are revealed by PENNI that are not visible in the diffraction-limited images. Parallel, intersected and branched structures combine to form complex networks. We note that while other super-resolution methods may provide comparable spatially resolved images, achievable timescales are temporally limited due to photobleaching. Resolving such networks in a nonbleaching manner can provide a unique opportunity to shed light on the temporal evolution of such structures and their resulting properties.

After resolving spatial heterogeneity with PENNI, we explored the temporal evolution of spatially resolved actin structures. An important criterium for temporal resolution is the response time of the precision optics. Switching the nanoIM between on and off states, we measured the turn-on response time to be 40ms and the turn-off response time to be 35ms. This is important because response time determines the timescale of dynamic activities that can be feasibly captured. The response time conceivably can be further decreased down to several milliseconds by patterning alignment surfaces and potentially down to nanoseconds using superachromatic liquid crystal molecules.

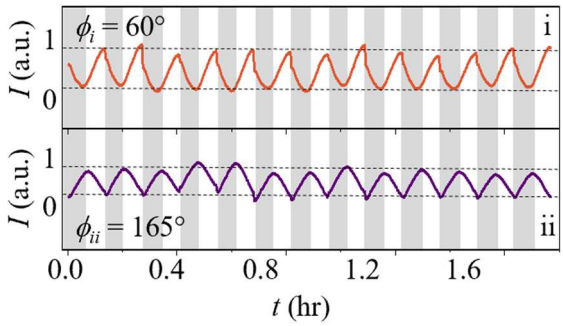

Figure 9. Nonbleaching nanoscopy is capable of long term & continuous analysis. PENNI-resolved image: i. Periodic scattering intensity *I(t)* over time corresponding to location i with phase of $\phi_i = 60°$ with respect to the transmission axis φ of precision optics. ii. Scattering intensity *I(t)* over time corresponding to location ii with phase of $\phi_i = 165°$ with respect to the transmission axis φ of precision optics.

We investigated the nonbleaching capabilities of PENNI by comparing scatterer-labeled bundles with fluorophore-labeled bundles (Figure 8). While fluorophores eventually photobleach, scatterers do not photobleach, enabling continuous time course endeavors. We observed parallel scatterer-labeled bundles can be spatially resolved using PENNI compared to the diffraction-limited image. In contrast, while parallel fluorophore-labeled bundles were initially resolved at time zero, fluorophore-labeled bundles immediately suffered from photobleaching shortly after continuous exposure to illumination. It is noteworthy to highlight that subdiffraction resolution was preserved under continuous analysis using PENNI, whereas in the control, subdiffraction capabilities were lost within seconds.

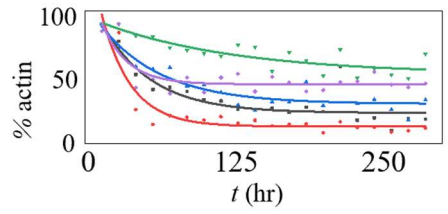

Figure 10. Nonuniform actin degradation rates below diffraction limit.

We investigated the nonbleaching capabilities of PENNI under long-term continuous analysis (Figure 9). We continuously modulated transmission intensity over extended time period of hours. Distinct periodic signals were distinguished from different locations caused by the different nanoscatterer orientations in the actin material. We observed no obvious fluctuation of the periodic signals with continuous analysis over extended time periods. This is important because the transmission

intensity must be stable over time in order to trace the temporal evolution of local rearrangements in macroscale materials.

Armed with a nonbleaching subdiffraction approach capable of broad timescales, we temporally mapped the ageing process using PENNI. We observed local rearrangements that were not visible in the diffraction-limited control and cannot be captured by other super-resolution techniques susceptible to photobleaching. Below the diffraction limit, we observed ageing bundles separated into parallel bundles over the course of days and shortened over the course of weeks (Figure 11). Quantification of biophysical parameter shows actin degradation rates are non-uniform below the diffraction limit (Figure 10). Under different temperatures, we continuously imaged the Brownian motion of the network. To measure subdiffraction temperature of protein actin, we traced to generate their random moving paths due to Brownian motion and analyzed the average moving distances.

Finally, we applied our method to biological cells where the strong scattering of cell structure often obstructs the observation of scatterers (gold nanorods). We cultured neuroblastoma (SY5Y) cells. Under dark-field imaging condition, the cellular structure exhibited strong scattering, resulting a poor signal-to-noise ratio for nanorods. After subtraction, the strong scattering background are effectively removed, where the nanorod signals previously buried within the background noise are revealed, enhancing the signal-to-noise ratio of the nanorods by as much as 65 fold. We demonstrated background suppression in terms of super resolution deconvolution. It can be seen that without background suppression, the deconvolution is not able to clearly resolve nanorods within close proximity due to excess noise. Additionally, the nanorods are not clearly visible with a strong background intensity. We demonstrated super-resolution deconvolution after background suppression clearly resolves nanorods.

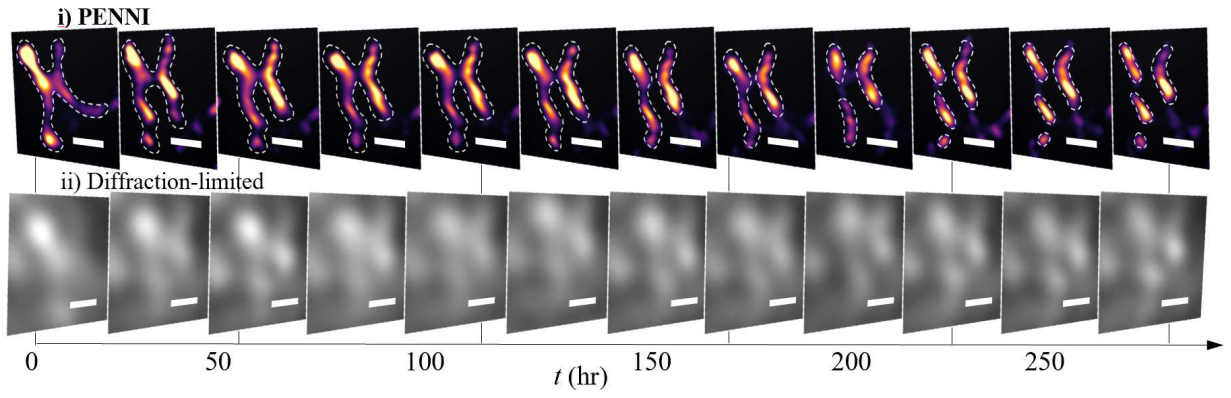

Figure 11. Long term, continuous subdiffraction imaging of ageing actin bundles (1.5 weeks).

PERSONNEL

Somin Eunice Lee (Assistant Professor)

Yipei Wang (Postdoctoral Fellow)

Yunbo Liu (Graduate Student)

Sam Carano (Graduate Student

Xintao Zhao (Graduate Student)

Gary Cui (Graduate Student)

Longshun Li (Graduate Student)

Hojae Lee (Graduate Student)

Christina Thantrakul (Graduate Student)

Wei-Kuan Lin (Graduate Student)

Zhijia Zhang (Graduate Student)

John Gregg (Graduate Student)

PATENTS

Lee, S.E., Wang, Y., Liu, Y., "Nano-Imaging system for resolving polarization-sensitive nanoparticles beyond diffraction limit," PCT Patent application # PCT/US2018/060128, 11/9/2018.

Lee, S.E., Liu, Y., Wang, Y. "Sub-diffraction imaging, coding and decoding of non-bleaching scatterers," U.S. Provisional application #62/657,045, 04/13/2018.

Lee, S.E., "Autonomous glare removal technique," U.S. Provisional application. 62/954,208-Conf. #6165, 2019

PUBLICATIONS

Liu, Y., Park, Y., Lee, S.E., "Thermo-responsive mechano-optical plasmonic nano-antenna," Appl. Phys. Lett., 108 (26), 013109, 2016

Liu, Y., Cui, G., Zhao, X., Lin, W., Da, A., Gregg, J., "Temporal heterogeneity of nanoenvironments by nonbleaching nanoscopy." Nature Nanotechnology, submitted

Lin, W., Cui, G., Burns, Z., Zhao, X., Liu, Y., Wang, Y., Ye, X., Park, Y., Lee, S.E., "Optically and structurally stabilized plasmo-bio interlinking networks for super-resolution," Advanced Materials Interfaces, submitted

Liu, Y., "Nonbleaching nanoscopy," Ph.D. thesis, in preparation

Liu, Y., Zhang, Z., Lin, W., Lee, S.E., "Ultraprecision imaging and manipulation by integrated nanoscopic correction," in preparation

Liu, Y., Zhao, X., Zhang, Z., Lee, S.E. "Intracellular high signal-to-noise ratio nano-imaging," in preparation

Liu, Y., Do, H., Flynn, H. Da, A. Gregg, J., Lee, S.E., "Multimodal autonomous glare removal," in preparation

Zhao, X., Cui, G., Gregg, J., Da, A., Lee, S.E., "Subdiffraction biomechanics by angular nonbleaching nanoscopy," in preparation

Liu, Y., Lee, S.E., "Review: Breaking the nonbleaching diffraction barrier," in preparation

Cui, G., Zhao, X., Lee, S.E., "Protocol: Nonbleaching nanoscopy of temporal dynamics," in preparation

CONFERENCE PRESENTATIONS

Lee, S.E., "Plasmonics-enabled single molecule and temperature detection," 90th ACS Colloids & Surface Science Symposium, Boston, MA, June 5-8, 2016

Lee, S.E., "Mechano-optical plasmonic nanoantenna," IEEE Optical MEMS & > Nanophotonics (OMN), Singapore, July 31- August 4, 2016

Wang, Y., Liu, Y., Lee, S.E., "High-speed nano-polarimetry for real-time plasmonic bio-imaging," SPIE Photonics West BiOS, San Francisco, CA, January 27 - February 1, 2018

Liu, Y., Wang, Y., Lee, S.E., "High spatial precision nano-imaging of polarization-sensitive plasmonic particles," SPIE Photonics West BiOS, San Francisco, CA, January 27 - February 1, 2018

Liu, Y., Lee, S.E., "High signal-to-noise, nonbleaching subdiffraction nanoscale imaging," SPIE Photonics West BiOS, San Francisco, CA, February 1-6, 2020

Cui, G., Lee, S.E., "Plasmonic subdiffraction imaging of single actin filament and actin network structures," SPIE Photonics West BiOS, San Francisco, CA, February 1-6, 2020

Lin, W., Lee, S.E., "Universal and quantitative measure of colloidal stability of plasmonic nanoparticles via comprehensive stability parameter method," SPIE Photonics West BiOS, San Francisco, CA, February 1-6, 2020

Gregg, J., Lee, S.E., “A framework for quantifying actin networks formed by different bundling techniques,” SPIE Photonics West BiOS, San Francisco, CA, February 1-6, 2020

Zhao, Z., Lee, S.E., “Quantitative super-resolution of time-resolved dynamics of actin via plasmonics,” SPIE Photonics West BiOS, San Francisco, CA, February 1-6, 2020